

Bypass transition delay using oscillations of spanwise wall velocity

Prabal S. Negi,^{1,*} Maneesh Mishra,² Philipp Schlatter,¹ and Martin Skote³

¹*Department of Mechanics, Linné FLOW Centre and Swedish e-Science Research Centre (SeRC), KTH Royal Institute of Technology, Stockholm SE-100 44, Sweden*

²*School of Mechanical and Aerospace Engineering, Nanyang Technological University, Singapore 639798*

³*School of Aerospace, Transport and Manufacturing, Cranfield University, Cranfield, MK43 0AL, United Kingdom*



(Received 10 June 2018; published 17 June 2019)

Large eddy simulations are performed to investigate the possibility of bypass transition delay in spatially developing boundary layers. An open loop wall control mechanism is employed which consists of either spatial or temporal oscillations of the spanwise wall velocity. Both spatial and temporal oscillations show a delay in the sharp rise in skin friction coefficient which is characteristic of laminar-turbulent transition. An insight into the mechanism is offered based on a secondary filtering of the continuous Orr-Sommerfeld-Squire (OSQ) modes provided by the Stokes layer, and it is shown that the control mechanism selectively affects the low-frequency penetrating modes of the OSQ spectrum. This perspective clarifies the limitations of the mechanism's capability to create transition delay. Furthermore, we extend the two-mode model of bypass transition proposed by T. Zaki and P. Durbin [*J. Fluid Mech.* **531**, 85 (2005)] to cases with wall control and illustrate the selective action of the wall oscillations on the penetrating mode in this simplified case.

DOI: [10.1103/PhysRevFluids.4.063904](https://doi.org/10.1103/PhysRevFluids.4.063904)

I. INTRODUCTION

An open loop wall forcing technique for turbulent drag reduction has been undergoing study for over two decades. The forcing technique takes a simple trigonometric form:

$$W_{\text{wall}} = W_m \sin(\omega t), \quad (1)$$

where W_{wall} is the spanwise velocity at the wall, ω is the angular frequency of the oscillation, and W_m is the maximum amplitude of spanwise wall velocity. The efforts started with direct numerical simulation (DNS) studies by Jung [1] and Akhavan [2] that reported large sustained turbulence suppression, accompanied by about 40% reduction in the skin friction coefficient in turbulent channel flows upon the introduction of an oscillatory wall motion. This control technique caught the attention of the community after a study by Baron and Quadrio [3], who reported a net positive energetic balance for the wall control technique, for small-amplitude oscillations. Several studies followed thereafter providing insights into different aspects of the control mechanism [4–19]. A qualitative equivalence between temporal and spatial wall oscillations for turbulence control was shown by Viotti *et al.* [20]. Quadrio *et al.* [21] extended the investigations to traveling wave-type wall control in their parametric study using DNS.

Eventually the focus branched off to study the impact of such wall oscillations on the transitional region. One route of transition from laminar to turbulent flows, generally referred to as bypass transition, involves the breakup of near-wall-boundary-layer streaks [22–25] which exist in laminar flows. Since the oscillating wall forcing attenuates the near-wall streaks in a turbulent region,

*negi@mech.kth.se

a similar effect on laminar streaks could possibly hinder their growth, thus causing a delay or possibly prevention of transition to turbulence. Transition to turbulence via the bypass route is known to occur through a two-stage process. The first stage involves the nonmodal amplification of disturbances, which leads to the formation of low-speed streaks in the boundary layer. In the second stage the low-speed streaks undergo secondary instability due to nonlinear interaction leading to streak breakdown and transition to turbulence [22–24]. The initial disturbances which amplify to form streaks are sometimes modeled using the continuous modes of the Orr-Sommerfeld-Squire (OSQ) operator. These modes have been used as a basis for the description of free-stream turbulence in several previous studies [22–29]. The shear filtering phenomenon causes the high-frequency modes of the continuous spectrum to have a vanishing component inside the boundary layer, while selectively allowing the low-frequency components to penetrate deeper into the boundary layer [29]. Zaki and Durbin [25] showed that both high- and low-frequency modes are necessary for bypass transition. However, only two modes (one high- and one low-frequency) suffice to create a transition scenario. The two-mode model of Zaki and Durbin [25] was confirmed by Schlatter *et al.* [24]. The existence of two possible breakdown mechanisms as elucidated in Ref. [30] was also shown by Schlatter *et al.* [24]. Experimental investigation of bypass transition by Mans *et al.* [31] using dye visualization shows pretransitional structures similar to those found in the numerical works of Brandt *et al.* [22]. More recently, Dong and Wu [32] have contended that a better way to model entrainment of free-stream disturbances is via the so-called linearized boundary-region equations which take into account the nonparallelism of the boundary layer. Nonetheless, the prediction of several numerical works based on the continuous OSQ spectrum predict flow features that are in good agreement with experimental results on bypass transition (see Ref. [24]).

While the quantitative picture of bypass transition remains incomplete, the qualitative picture points towards the secondary instability of low-speed streaks in laminar boundary layer. Since spanwise oscillations suppress streak formation in turbulent boundary layers, their effect was then studied in pretransitional boundary layers. Ricco [33] demonstrated in a linearized study that large attenuation of laminar streaks under the effect of steady spatial oscillations is possible. Hack and Zaki [28] show an enhancement of the shear filtering process in another linearized study with time harmonic wall oscillations. The shear filtering process also assumed a time dependence due to the temporal variation of the base flow [28]. Jovanovic [34] studied small-amplitude oscillations in transitional Couette and Poiseuille flows and showed large ensemble energy density reduction. Using a newly developed nonlinear variational method, Rabin *et al.* [35] showed that the minimum initial disturbance to trigger transition to turbulence is substantially increased in plane Couette flow in the presence of temporal spanwise wall oscillations. Negi *et al.* [36] performed a DNS of a single low-speed streak under the influence of spatial wall oscillations and showed a delay in the characteristic rise of skin friction during transition. Berlin’s Ph.D. work [37] predates all these studies, in which he studied temporal wall oscillations applied on oblique wave transition as well as transition due to random noise and showed that a large transition delay is possible. Hack and Zaki [38] performed a DNS study with temporal oscillations on pretransitional boundary layers and showed transition delay for flows with free-stream turbulence.

These recent studies have shown promising signs of creating significant transition delay using wall oscillations. In the current study, large eddy simulations (LESs) have been performed to further investigate the effectiveness of both spatial and temporal oscillations of spanwise wall velocity in delaying bypass transition. Detailed studies focusing on temporal oscillations for pretransitional boundary layers can be found in Refs. [28,38,39]. The current work focuses on spatial oscillation of the spanwise wall velocity while some simulations for temporal oscillation are also performed for the purpose of comparison between the two types of wall control.

II. NUMERICAL SETUP

The code used in this study was developed at KTH, Stockholm [40]. It is based on a pseudo-spectral method to solve the three-dimensional, time-dependent, incompressible Navier-Stokes

equations. The algorithm uses Fourier representation in the streamwise and the spanwise directions, while Chebyshev polynomials are employed in the wall-normal direction. The algorithm uses a pseudospectral treatment of the nonlinear terms with multiplications of those terms calculated in physical space to avoid the sum of convolution terms. Fast Fourier transform (FFT) is used for the transformation between physical and spectral space. For the time advancement of the nonlinear terms, a four-step, low-storage, third-order Runge-Kutta method is used, while a second-order Crank-Nicolson method is used for the advancement of the linear terms. Aliasing error from the evaluation of nonlinear terms is removed by the 3/2 rule for FFT calculations in wall-parallel planes, while in the wall-normal direction, increasing spatial resolution has been found to be more efficient than dealiasing. A spatial technique is necessary in order to appropriately account for the streamwise development of the boundary layer. The requirement is combined with the periodic boundary condition in the streamwise direction by the use of a “fringe region.” This region is implemented at the downstream end of the computational domain, where a volume forcing is added to the flow such that the flow is forced to a desired inlet solution. The ADM-RT model is used for the LESs, which is based on the approximate deconvolution procedure [41]. The model has previously been used in several studies of wall-bounded flows [42–44] and has been shown to accurately simulate transitional flows [42].

The length scale used for the normalization is based on the inlet displacement thickness, δ_o^* , the velocity scale used is the inlet free-stream velocity, U_∞ , and time is normalized using δ_o^*/U_∞ . The displacement thickness-based Reynolds number $Re_{\delta_o^*} = 300$ at the inlet has been used for all cases unless otherwise specified. The computational domain for the simulation was set at 2000, 180, and 60 units in the streamwise, spanwise, and wall-normal directions, respectively, based on the inlet displacement thickness δ^* . The fringe region was set to 100 units right before the end of the computational domain. The resolution of the study was set to 512 and 128 Fourier modes in the streamwise and spanwise directions, respectively, with 121 points in the wall-normal direction. The nonlinear terms are evaluated in physical space on a finer grid of 768×192 collocation points in the wall-parallel directions corresponding to the 3/2 rule. The setup is the same as the one used in Ref. [45] to study the interaction of noise in the boundary layer with streamwise streaks. An identical setup is used in Ref. [46] where an extensive validation of the computational setup is performed, showing good agreement between the shape of the Tollmien-Schlichting (TS) waves with linear stability theory as well as streamwise evolution of TS waves as predicted by parabolic stability equations. The effect of free stream was added as a superposition of the continuous modes of the OSQ spectrum prescribed at the inlet, which can be described mathematically by

$$u_j = \sum_{\alpha} \sum_{\beta} \sum_{\omega} \phi(\alpha, \beta, \Omega) \tilde{u}_j(y, \alpha, \beta, \Omega) e^{i(\alpha x + \beta z + \Omega t)}, \quad (2)$$

where \tilde{u}_j is the solution of the OSQ equations for the boundary layer at inlet Reynolds number, and ϕ is a scaling factor for the specified wave-number combination. In order to discretize the free-stream turbulence spectrum the wave-number space is divided into concentric spherical shells with points selected from each shell such that the equivalent spectrum is isotropic. Care is taken to eliminate special cases such as standing waves. The selection is performed for 20 discrete shells amounting to a total of 200 spectral modes for the free-stream turbulence. The energy distribution, and thus the scaling ϕ , of the spectrum is created in accordance with the von Kármán spectrum for homogeneous turbulence, which is of the form

$$E(k_{fst}) \propto \frac{k_{fst}^4}{(C + k_{fst}^2)^{17/6}}. \quad (3)$$

A detailed description of the calculation of free-stream turbulence spectrum can be found in Ref. [47]. The same procedure was used for the generation of free-stream modes in Refs. [22,24]. A similar procedure has also been used for generating grid turbulence for the numerical simulations

TABLE I. Streamwise position x and Re_x conversion.

x	0	200	300	400	1200	1800	2000
Re_x	30 000	90 000	120 000	150 000	390 000	570 000	630 000

of wind turbines [48]. The OSQ spectrum was calculated with a turbulence intensity (Ti) of 4.7%, which is the same as the one used in Ref. [22]. A reference case for transition due to free-stream turbulence without wall control was also performed. The same spectrum was used as the inlet condition for all subsequent cases with wall control. Comparisons of all wall control cases are made with this reference case.

The simulations were run for 15 000 time steps. All statistics up till 4000 time steps were discarded, and values from $t = 4000$ –15 000 were used to compute all averaged quantities. The statistical quantities presented herein are spanwise averaged unless specifically mentioned otherwise.

For specifying the streamwise location, both x and Re_x values are used as appropriate. Since the computational box starts at $x = 0$, the relation between the two variables is given by $Re_x = (Re_{\delta_0^*}/1.721)^2 + Re_{\delta_0^*}x$. For convenience, commonly used streamwise positions are specified in Table I.

III. SPATIAL OSCILLATIONS

Steady spatial oscillations of spanwise wall velocity are implemented as described by

$$W_{\text{wall}} = W_m \sin(kx), \quad (4)$$

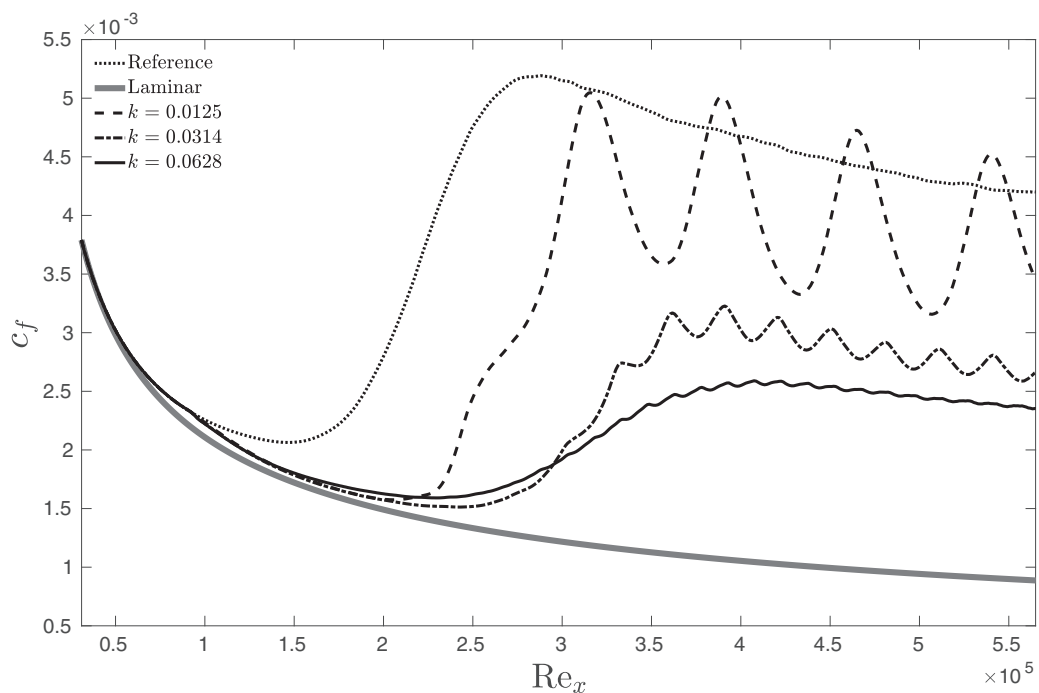


FIG. 1. Friction coefficient c_f showing transition delay for wall oscillations with different wave numbers ($k = 0.0125, 0.0314, 0.0628$) and $W_m = 0.9$.

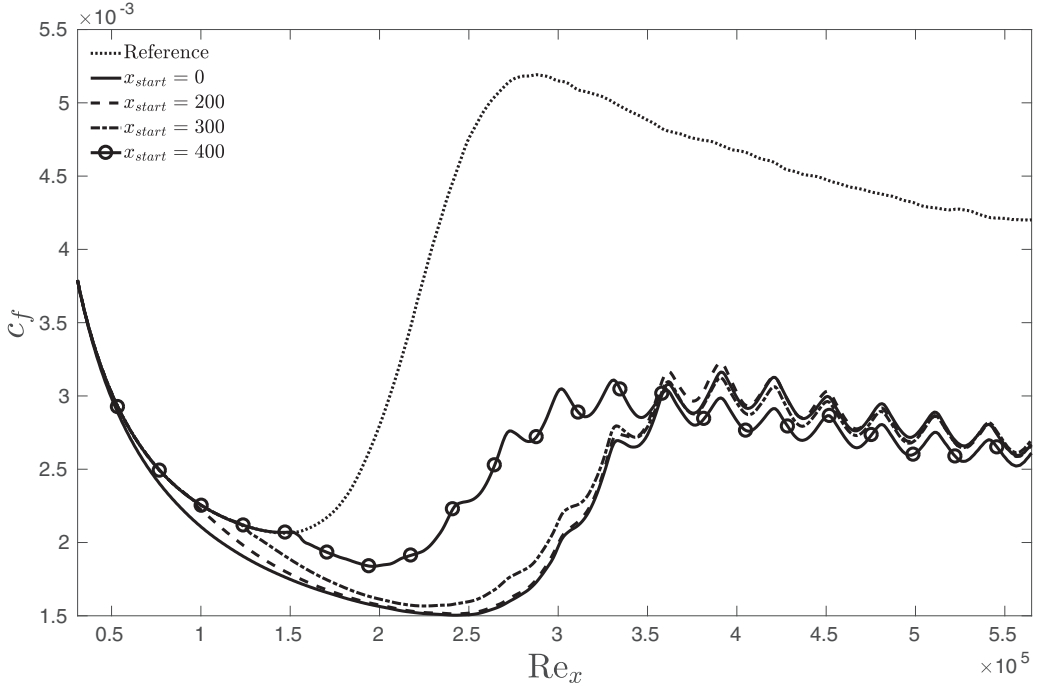


FIG. 2. Transition delay for different start points of oscillation ($x_{\text{start}} = 0, 200, 300, 400$). The start locations correspond to $\text{Re}_x = 0.3, 0.9, 1.2,$ and 1.5×10^5 , respectively.

where k is the wave number of the streamwise oscillations. The wall control region spans from $x_{\text{start}} = 200$ to $x_{\text{end}} = 1800$, where x_{start} marks the start of the wall oscillations while x_{end} denotes the end. This corresponds to approximately $\text{Re}_x = 0.9 \times 10^5$ and $\text{Re}_x = 5.7 \times 10^5$, respectively. The start of the oscillations was kept upstream of the minimum observed in the c_f curve for the reference case with no wall control, i.e., before transition. Following the setup of Ref. [13] the amplitude of wall oscillations W_m is set to 0.9. Figure 1 shows the evolution of skin-friction coefficient c_f under the effect of wall control with different wave numbers. The skin-friction coefficient c_f is defined as

$$c_f(x) = \frac{1}{(z_{\text{max}} - z_{\text{min}})} \int_{z_{\text{min}}}^{z_{\text{max}}} \frac{\tau_w(x, z)}{\frac{1}{2}\rho U_{\infty}^2} dz, \quad (5)$$

where

$$\tau_w = \mu \left(\frac{\partial u}{\partial y} \right)_{y=0}. \quad (6)$$

For quantitative comparisons, the point of transition is defined as the spatial minimum in c_f , and the delay in transition defined by the difference in the point of transition between the oscillating wall and reference cases.

Figure 1 shows the c_f curve for the reference and control cases with different wave number k . The initial change of c_f is almost the same for all cases, with the values decreasing at the onset of wall oscillation. A visible delay in transition is observed for all cases, but the trend is nonmonotonic. The lowest wave number, $k = 0.0125$, creates the least delay in transition with $\Delta \text{Re}_x = 58\,594$. This also has the least suppression of turbulence in the fully turbulent regime. $k = 0.0314$ causes the largest transition delay of $\Delta \text{Re}_x = 94\,922$, while $k = 0.0628$ creates a delay of $\Delta \text{Re}_x = 82\,031$. It is worth noting that the drag reduction in the fully turbulent regime for the wall control case of

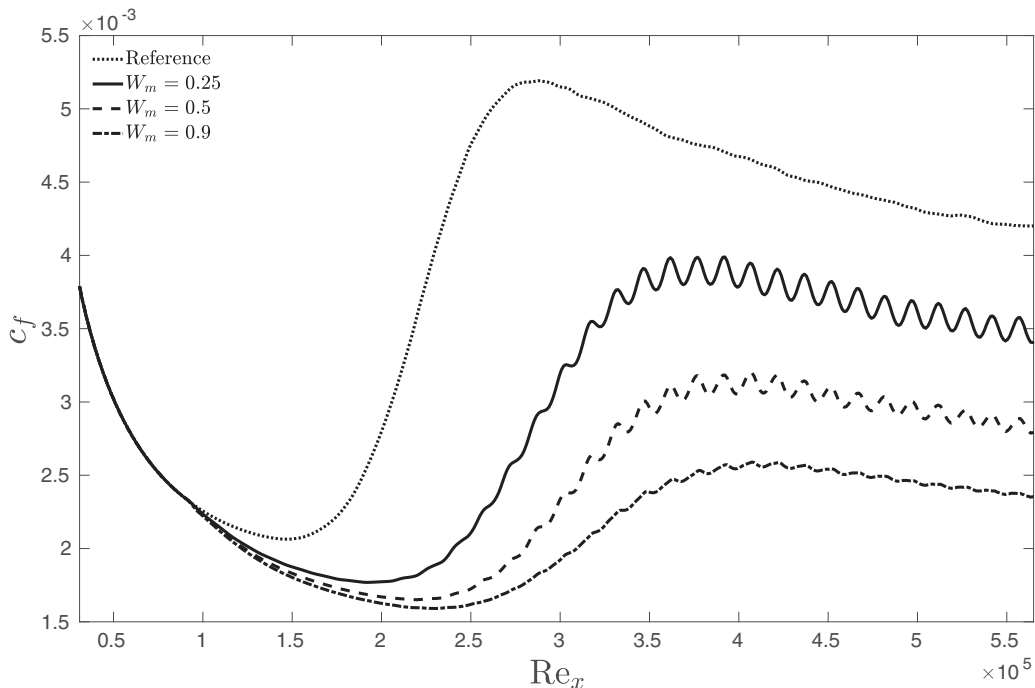


FIG. 3. Transition delay for varying amplitude for $k = 0.0628$.

$k = 0.0314$ is lower than that for $k = 0.0628$. For transition delay, however, $k = 0.0314$ creates a slightly larger transition delay as compared to $k = 0.0628$. Therefore the optimum wave number for drag reduction and transition delay may not coincide.

The wall control mechanism was further tested by changing the start location (x_{start}) of the oscillation for the optimal wave number of $k = 0.0314$. The start of the control was set at $x_{\text{start}} = 0, 200, 300,$ and 400 , corresponding to $\text{Re}_x = 0.3, 0.9, 1.2,$ and 1.5×10^5 . Figure 2 shows the effect of x_{start} on transition delay. In general, an upstream movement of the start of wall control increases the transition delay that can be achieved. For $x_{\text{start}} = 400, 300,$ and 200 the transition delays achieved were $\Delta \text{Re}_x = 49\,218, 77\,344,$ and $94\,922$, respectively. However, the gain in transition delay due to upstream movement of the x_{start} saturates, with transition delay observed for $x_{\text{start}} = 0$ ($\Delta \text{Re}_x = 96\,094$) being very close to the value observed for $x_{\text{start}} = 200$ ($\Delta \text{Re}_x = 94\,922$).

Changing the amplitude of the spatial oscillations again has a nonmonotonic effect on transition delay. For $k = 0.0628$ an increase in oscillation amplitude caused a larger transition delay (Fig. 3). For $k = 0.0125$ transition delay increases as the amplitude is increased from $W_m = 0.25$ to $W_m = 0.5$. However, a further increase in the amplitude to $W_m = 0.9$ reduces the transition delay (Fig. 4). In temporal wall oscillation cases the cross-flow instability can be triggered at high wall-oscillation amplitudes, which explains the existence of an optimum amplitude for transition delay [39]. Possibly a similar phenomenon occurs for the spatial oscillations.

The evolution of the flow in case of wall control in the transitional region can be compared with the case of flow control in fully turbulent flows. Figure 5 shows the skin friction coefficient development in the two cases of pre- ($x_{\text{start}} = 200$) and post- ($x_{\text{start}} = 1000$) transition wall control, plotted against Re_{δ^*} . For the posttransition case, the start of wall control is set after the maxima of the c_f curve of the reference case. The c_f curves for the two cases almost coincide, suggesting that flow eventually converges to the same state independently of the start location of wall control.

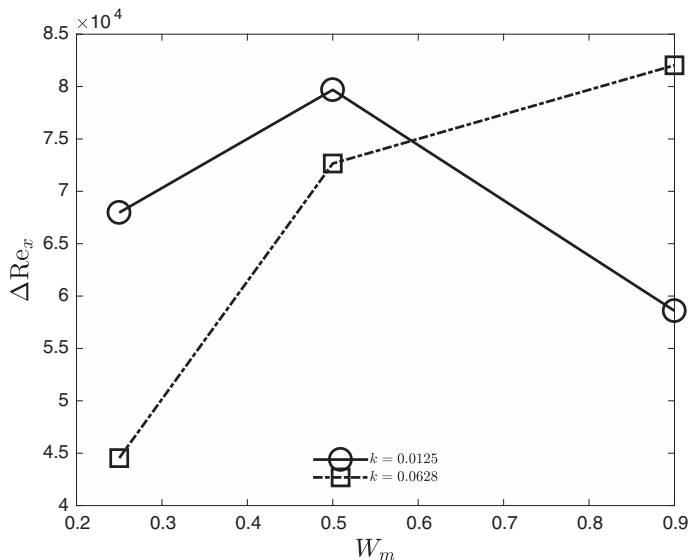


FIG. 4. Transition delay for varying amplitude.

The wall control is also tested for a case of different turbulence intensity. The inlet turbulence spectrum is normalized to a turbulent intensity of 3.5%, and wall control is implemented from $x_{\text{start}} = 400$. Figure 6 compares the evolution of c_f for the two different turbulent intensities and their respective wall control cases. As we would expect, transition delay is seen even for the low-intensity case with the delay being larger ($\Delta Re_x = 63\,281$) in the presence of control for $Ti = 3.5\%$ than for the case of $Ti = 4.7\%$ ($\Delta Re_x = 49\,219$).

Qualitatively, bypass transition is known to occur via a two-stage process of nonmodal amplification of disturbances and then nonlinear interaction of continuous modes of the OSQ spectrum leading to streak breakdown [22–25]. Previous studies [28,33,36] have shown that wall oscillation substantially reduces the magnitude of peak fluctuations in the laminar boundary layer, which will also be demonstrated in a later section. The magnitude of reduction has been reported to be as high as 90% [33,36]. Hence the wall control technique should create a substantial transition delay if implemented just upstream of the transition location. With this in mind, the oscillation is applied in a short region ($x = 200\text{--}400$) right before the transition location in the reference case. Figure 7 shows the c_f change in case of a short pretransitional control region, comparing it with a case of an extended control region. Indeed, a relatively large transition delay ($\Delta Re_x = 42\,188$) can be achieved with a short pretransitional wall control as compared to the case when the control region extends over a large region.

IV. TEMPORAL OSCILLATIONS

In the control of fully turbulent flows via spanwise wall oscillations, temporal and spatial oscillations are seen to be largely analogous [15,20], with spatial oscillation having a slightly better energy savings. The optimum wave numbers for spatial oscillations and the optimum angular frequency for temporal oscillations (in fully turbulent flows) have been shown to be the same under space-time conversion [20]. Temporal oscillations are therefore tested for their ability to create transition delays, similar to ones observed in the spatial oscillation cases. Temporal oscillation of the spanwise velocity at the wall as described by Eq. (1) was implemented with the control region spanning from $x_{\text{start}} = 300$ to $x_{\text{start}} = 1800$.

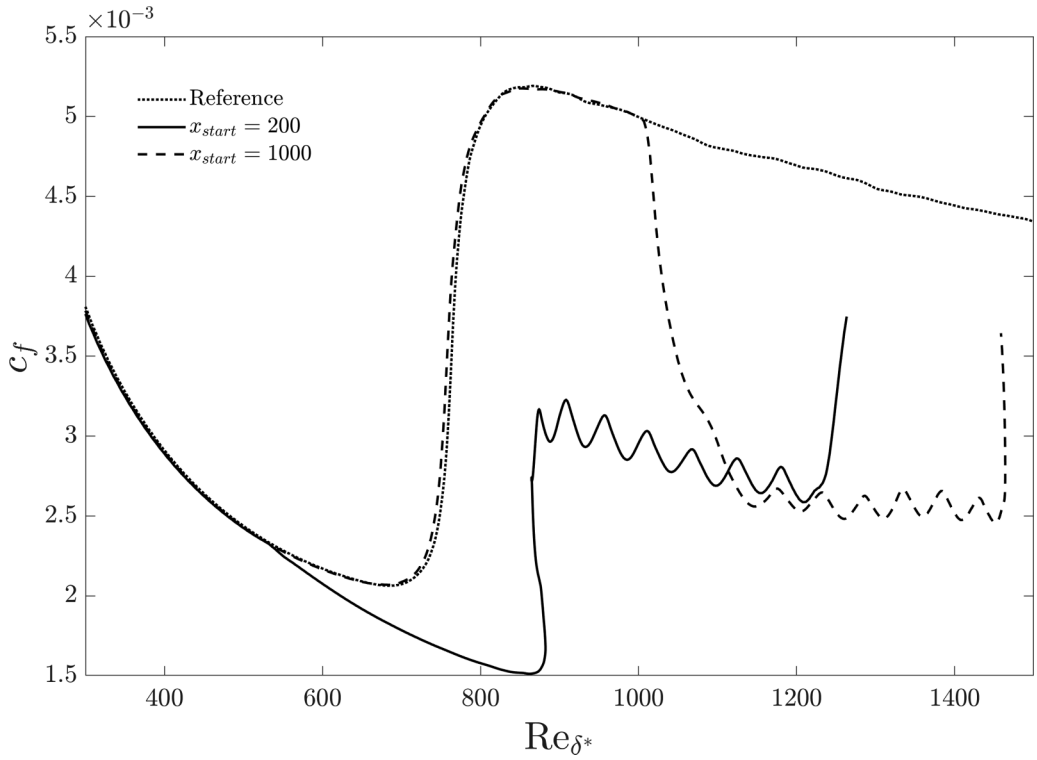


FIG. 5. Coefficient of skin friction development for pre- and posttranslational wall control.

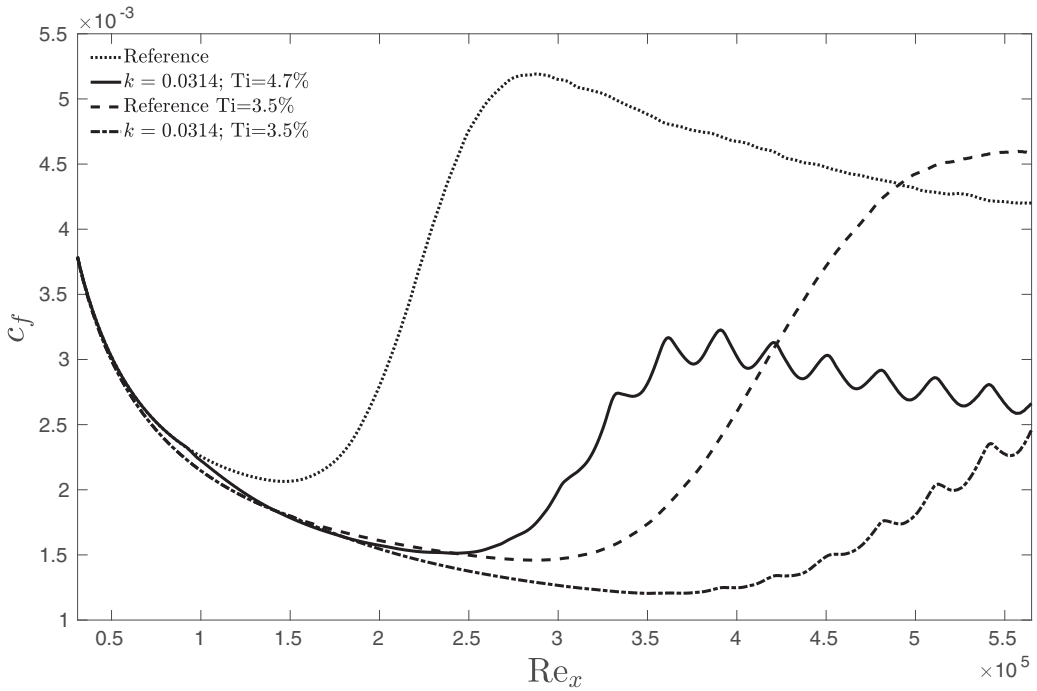


FIG. 6. Transition delay for different inlet turbulence intensities ($k = 0.0314, Re_{x_{start}} = 0.9 \times 10^5$).

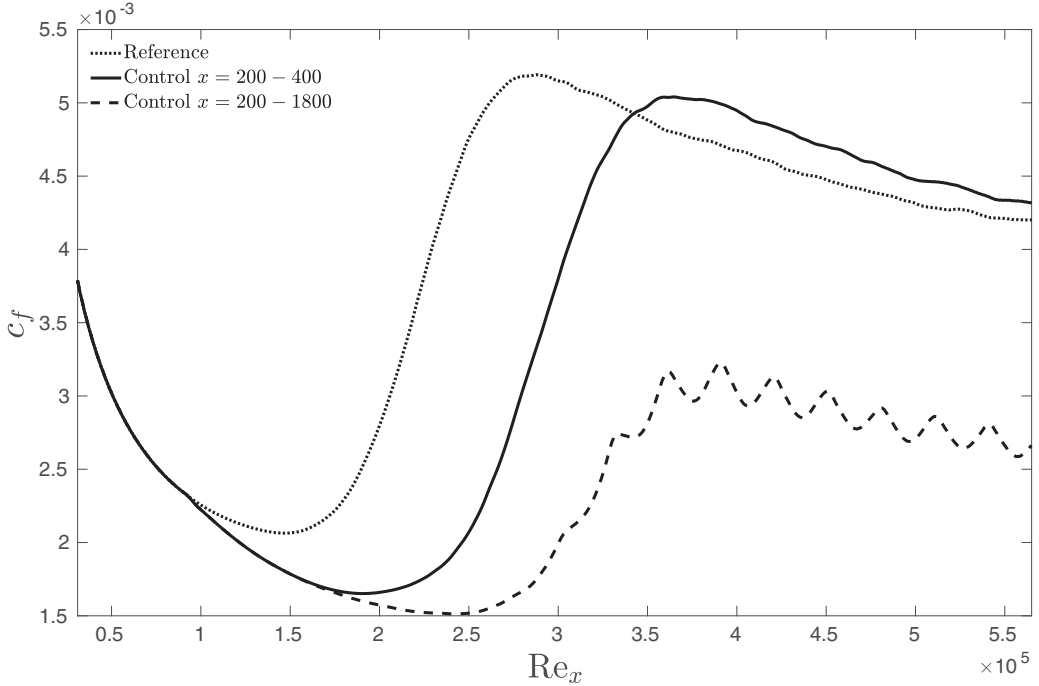


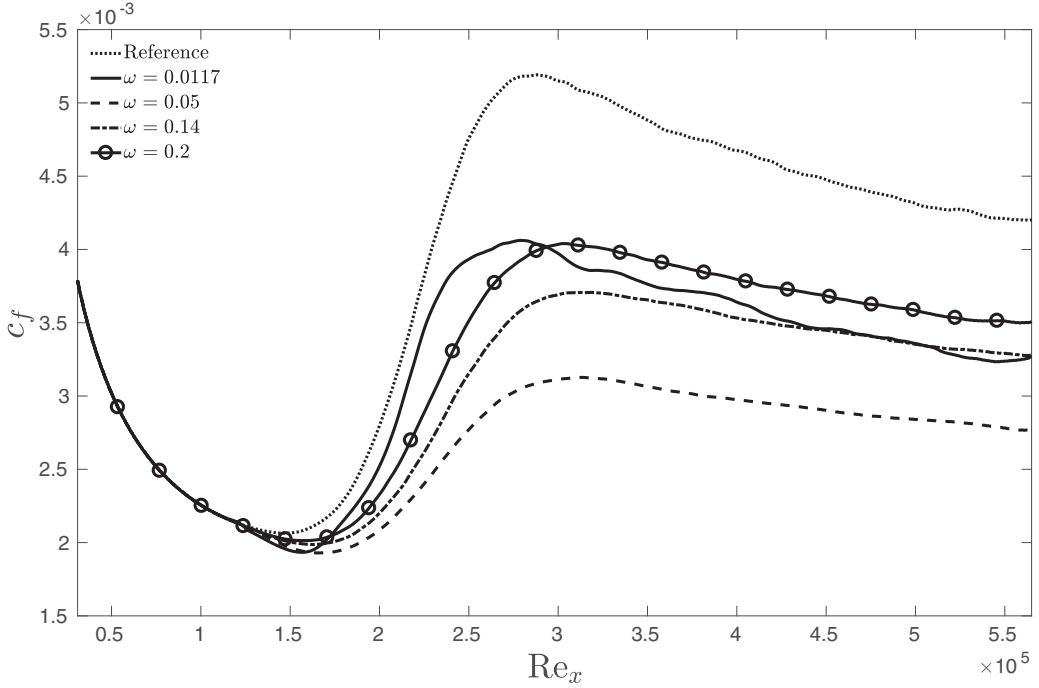
FIG. 7. Transition delay with a short pretransitional wall control ($k = 0.0314$). The control regions correspond to $\text{Re}_x = 0.9\text{--}1.5 \times 10^5$ and $\text{Re}_x = 0.9\text{--}5.7 \times 10^5$.

Figure 8 shows the evolution of the skin friction coefficient under the effect of temporal wall control. Four different oscillation frequencies were used while keeping the maximum spanwise wall velocity constant at $W_m = 0.9$. The frequency $\omega = 0.05$ caused the largest delay in transition, which amounted to $\Delta\text{Re}_x = 18\,750$. Subsequent higher frequencies showed a much lower capacity for transition delay.

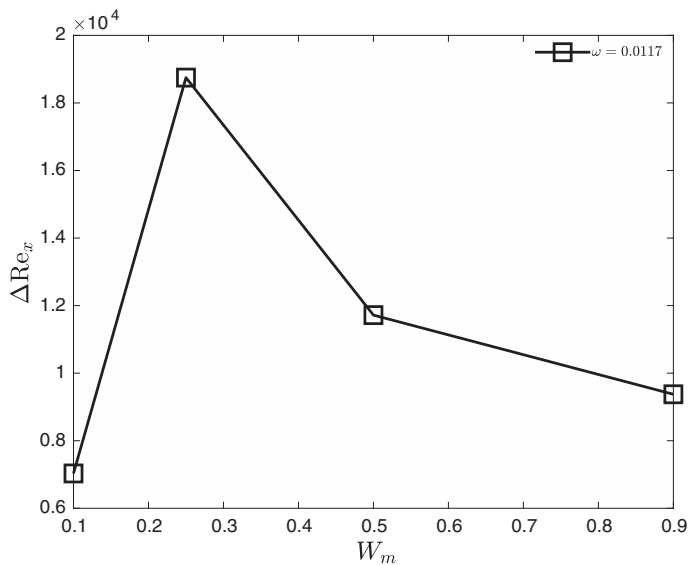
Varying the amplitude for a single oscillation frequency ($\omega = 0.0117$) reveals an optimum amplitude for transition delay (Fig. 9), similar to the case of control with spatial oscillations. A similar result for optimum oscillation amplitude for temporal wall oscillations is reported in Refs. [37,38].

When changing the start of wall control to an upstream position a larger transition delay is achieved. Figure 10 shows the c_f curve for $\omega = 0.0117$ with $W_m = 0.25$ for two different x_{start} locations. For $x_{\text{start}} = 300$ the oscillatory control causes a transition delay of $\Delta\text{Re}_x = 18\,750$. On the other hand, moving the start of wall control to the beginning of the simulation box ($x_{\text{start}} = 0$) causes a much larger transition delay of $\Delta\text{Re}_x = 49\,219$.

The results of the temporal oscillation cases show a similar trend to those of the spatial oscillation case. In addition, results of transition delay reported in Ref. [38] show a similar behavior with a nonmonotonic trend in transition delay observed for both oscillation frequency (ω) and amplitude (W_m). However, in the same study a large extent of transitional region is reported. In our current work, we do not see such large extensions of the transitional region. In particular, the case of $\omega = 0.0117$ has a frequency which is close to the optimum frequency found in Ref. [38] (referred to as $T = 200$ in Ref. [38]). Figure 10 shows the c_f curve for the case with $W_m = 0.25$ and with the wall control starting from the beginning of the computational domain ($x_{\text{start}} = 0$). The setup is thus very similar to the optimum setup reported in Ref. [38]; however, no large extensions of the transitional region can be observed. Bypass transition, being a nonlinear process, is highly dependent on the spectrum content of free-stream turbulence [22] as well as the turbulence intensity


 FIG. 8. Transition delay for temporal oscillation cases ($W_m = 0.9$).

(Ti). The simulations of Hack and Zaki [38] were performed with $Ti = 3.0\%$ with a slightly lower inlet Reynolds number of $Re_{\delta^*} \approx 276$ as compared to the current study where $Ti = 4.7\%$ and $Re_{\delta^*} \approx 300$. As already seen in the section for spatial oscillations (Fig. 6), for the same wall control parameters, a larger transition delay can be achieved for lower Ti cases. An extended


 FIG. 9. Transition delay for $\omega = 0.0117$ at different oscillation amplitudes.

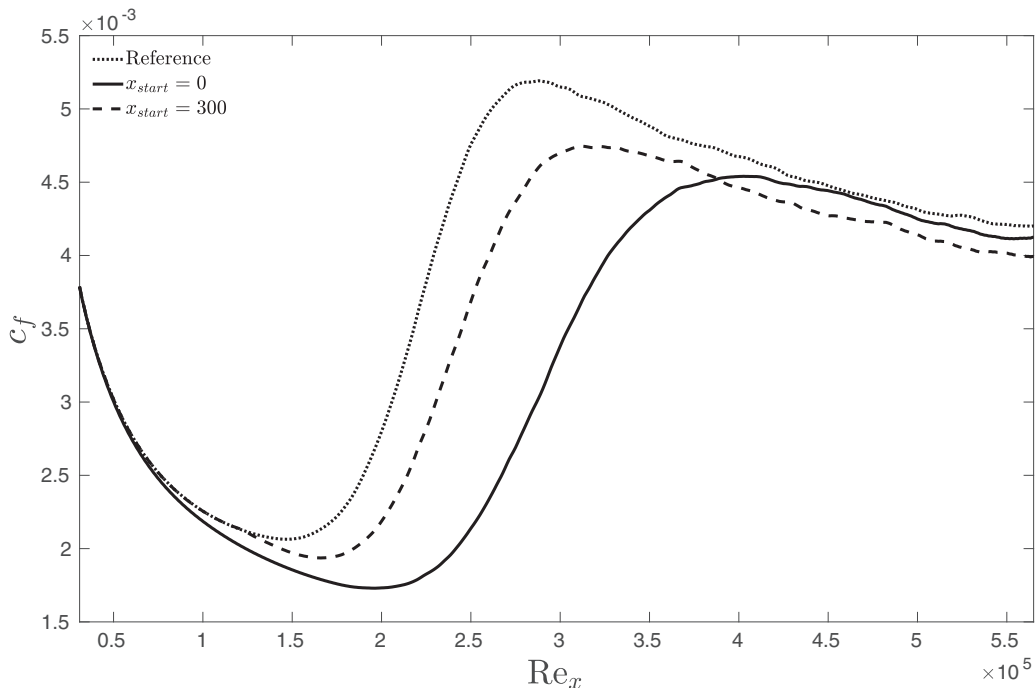


FIG. 10. Transition delay for temporal oscillation with $W_m = 0.25$ and $\omega = 0.0117$ and different x_{start} locations ($Re_x = 0.3$ and 1.2×10^5).

transitional region could be the artifact of lower turbulence intensity, leading to a slower nonlinear growth.

V. TURBULENT QUANTITIES AND STOKES LAYER HEIGHT

In the previous two sections, the results for the transition delay were reported, without an attempt to explain the various factors that influence the drag-reduction mechanism. Therefore, in order to better understand the transition delay mechanism, we take a closer look at the fluctuation intensities and the Stokes layer generated by the spanwise wall oscillations. The results and analysis in this section are presented using the spatial oscillation cases, with the expectation that temporal cases would have qualitatively similar underlying mechanisms. Peak streamwise fluctuations (u_{rms}^{max}) for the different wave-number cases (with $W_m = 0.9$, with control region spanning $Re_x = 0.9 - 5.7 \times 10^5$) are plotted in Fig. 11. With the onset of oscillatory wall control, the peak u_{rms} values initially decrease. However, after reaching a minimum value the peak fluctuation intensities start growing again, and the flow eventually transitions to turbulence. For the lowest wave number $k = 0.0125$, the rise in peak streamwise fluctuations roughly coincides with the transition location. However, for the other wave-number cases, the peak streamwise fluctuations start growing substantially upstream of their respective transition locations. This regrowth of fluctuation intensities was not seen in the works of Negi *et al.* [36], where the authors considered the effect of control on a single streak. After transition, u_{rms}^{max} stabilizes to become oscillatory within the wall control zone with the mean value being lower than the reference case values.

It is instructive to look at the streamwise development of the wall-normal location of peak streamwise velocity fluctuations within the boundary layer (Fig. 12). A general pattern can be observed for the individual cases, where the wall-normal location of the peak streamwise fluctuations has two distinct regions. First is the region upstream of the transition point, where

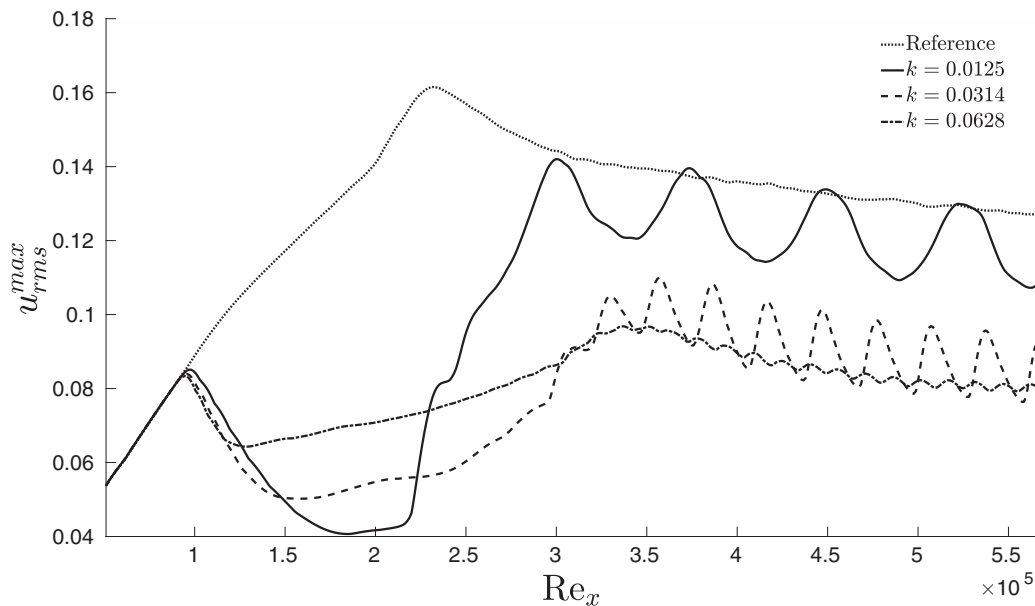


FIG. 11. Peak streamwise fluctuations u_{rms}^{max} for different wave-number cases. The control region starts at $Re_x = 0.9 \times 10^5$.

this peak location is at $y \approx 2.0$ – 2.5 for the reference simulation, and at $y \approx 3.0$ – 4.5 for the control cases. The second region is after flow transition, where the peak locations for both the reference and control cases move much closer to the wall. A wall-normal profile of streamwise velocity

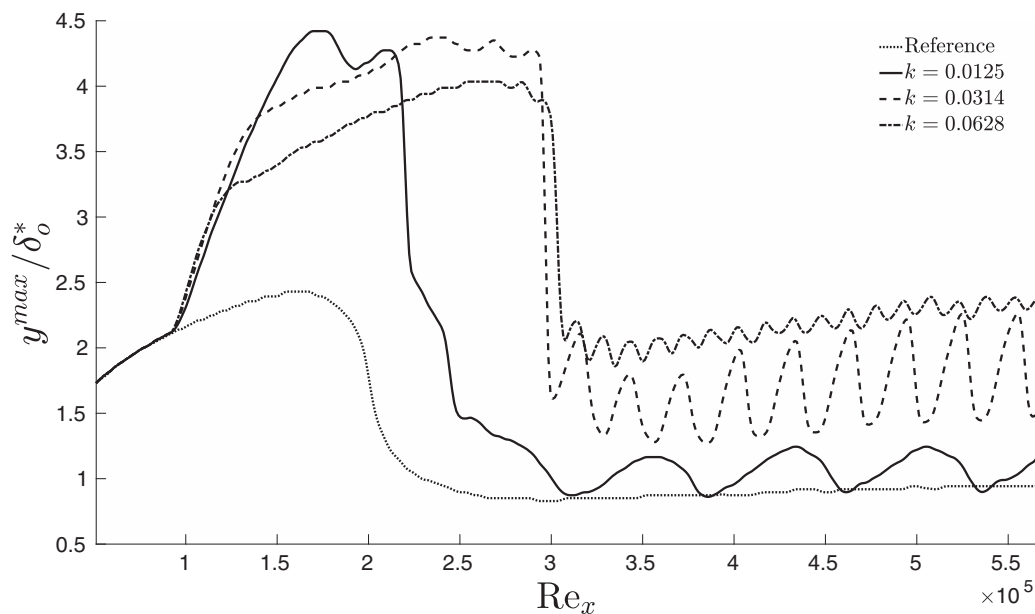


FIG. 12. Wall normal location of peak streamwise velocity fluctuations u_{rms}^{max} for different wave-number cases.

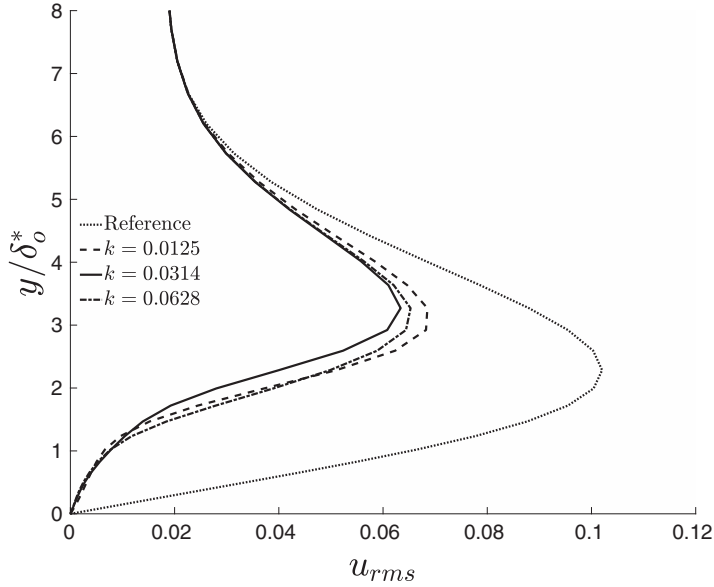


FIG. 13. Wall-normal profile of streamwise velocity fluctuations u_{rms} for different wave-number cases at $x = 300$. Note that the wall-normal coordinate is scaled using the inlet displacement thickness δ_o^* .

fluctuations at $x = 300$ (before transition) can be seen in Fig. 13 for different wave-number cases. The profile retains the general structure of the reference case, however, with lower intensity and its peak intensity location shifted away from the wall. The region very close to the wall fluctuation intensity is highly attenuated as compared to the reference case. A comparison of a snapshot of the instantaneous flow at $x = 300$ (Fig. 14) shows the effect of the imposed wall control. In the reference case the footprint of the streaks is clearly observed to go down to the wall, while in the case of wall control, the region close to the wall is nearly devoid of fluctuations. The streaky structures are seen farther away from the wall, in the region $y \approx 2-6$. From the instantaneous snapshots and the wall-normal profile, it appears that the mechanism of streak formation is still active with a lower intensity and with the location of streak formation shifted slightly away from the wall. An explanation of this outward shift can be found when one looks at the Stokes layer profile.

The averaged Stokes layer profile for spatial wall oscillations of the type given by Eq. (4) can be evaluated analytically both for turbulent and laminar flows under the assumption of a thin Stokes layer compared to the boundary layer thickness. The averaged Stokes profile is given by [13,20]

$$W(x, y) = \frac{W_m}{\text{Ai}(0)} \Re \left[(e^{ikx - i\pi/2}) \text{Ai} \left(-\frac{iy}{\delta_x} e^{-i4\pi/3} \right) \right], \quad (7)$$

where

$$\delta_x = \left(\nu^{-1} k \frac{\partial u}{\partial y}_{y=0} \right)^{-1/3}, \quad (8)$$

and Ai is the Airy function of the first type.

Figure 15(a) shows the Stokes layer profile for different wall phases of oscillation, while Fig. 15(b) shows the boundary layer profile (at $x = 300$) for the reference case as well as for wall control cases. The δ_{99} height of the boundary layer is at $y = 8.2$, whereas the Stokes layer is seen to substantially diminish at $y = 2$ and the oscillation amplitude is near zero at about $y = 3$. It is therefore in the region where the Stokes layer has a negligible effect ($y > 2$) that the mechanism

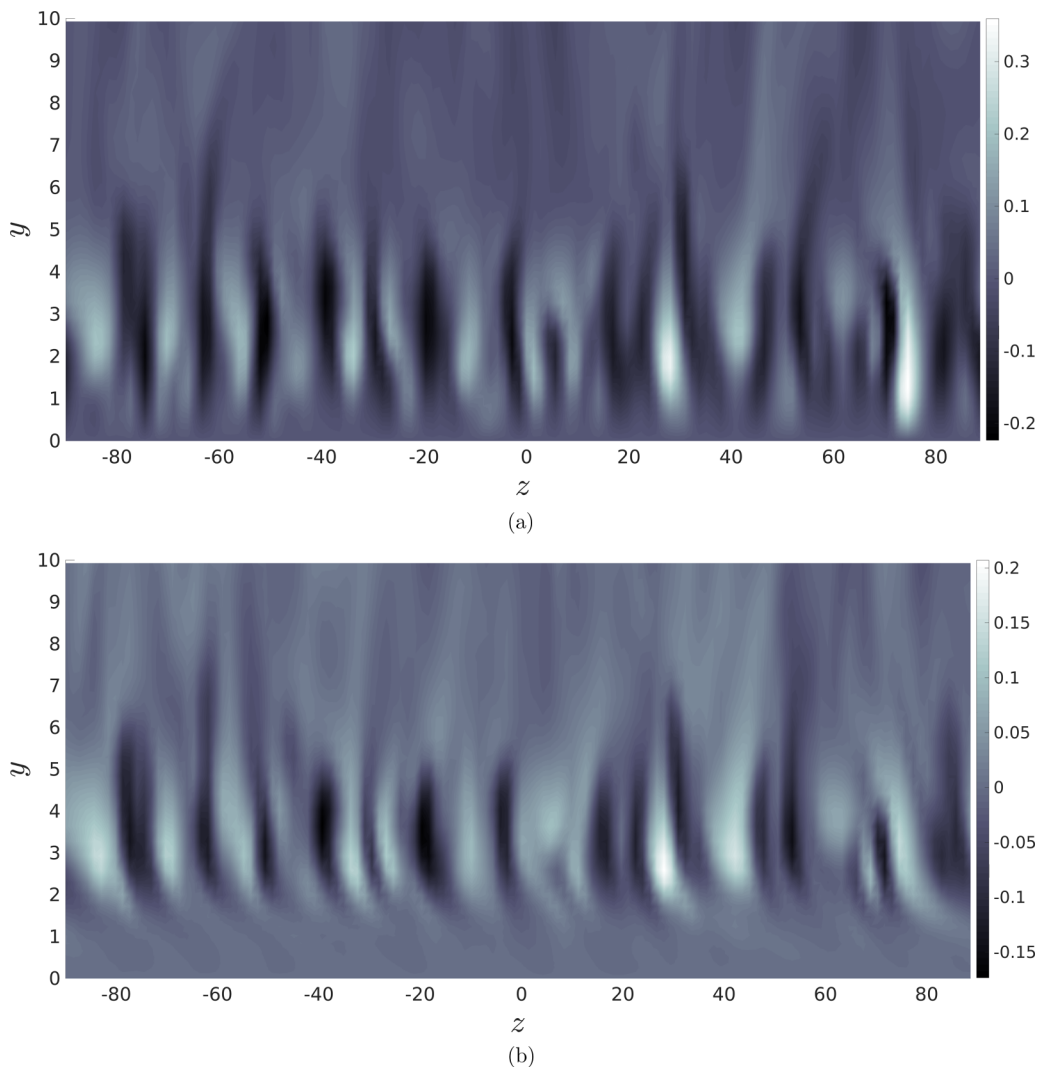


FIG. 14. A near-wall y - z plane at $x = 300$ of the instantaneous streamwise velocity with the spanwise mean subtracted from the instantaneous values, for (a) the reference case and (b) wall control with $k = 0.0314$, $W_m = 0.9$. Dark (light) regions represent velocity deficit (excess).

of streak formation becomes dominant again and we start to see the streaky structures which are characteristic of shear flows. Also important to note is that the mean streamwise velocity profile does not change significantly despite the disappearance of the streaks close to the wall.

The results can be interpreted in the framework of the continuous modes of the OSQ equation whereby the formation of streaks is the result of the incomplete cancellation of the Squire modes within the boundary layer. In the presence of three-dimensional disturbances, the Squire equation is forced by the Orr-Sommerfeld modes. A single Orr-Sommerfeld mode forces all Squire modes by distorting the mean vorticity. However, in the free stream the Squire equation is not forced due to the absence of mean shear, and there is consequently no source term for wall-normal vorticity. Thus, in the free stream the Squire modes must sum up to zero [25,49]. On the other hand, the existence of shear in the boundary layer has twin effects. First, the Squire equation is now forced by the three-dimensional Orr-Sommerfeld modes. Second, the process of shear-filtering causes a variation

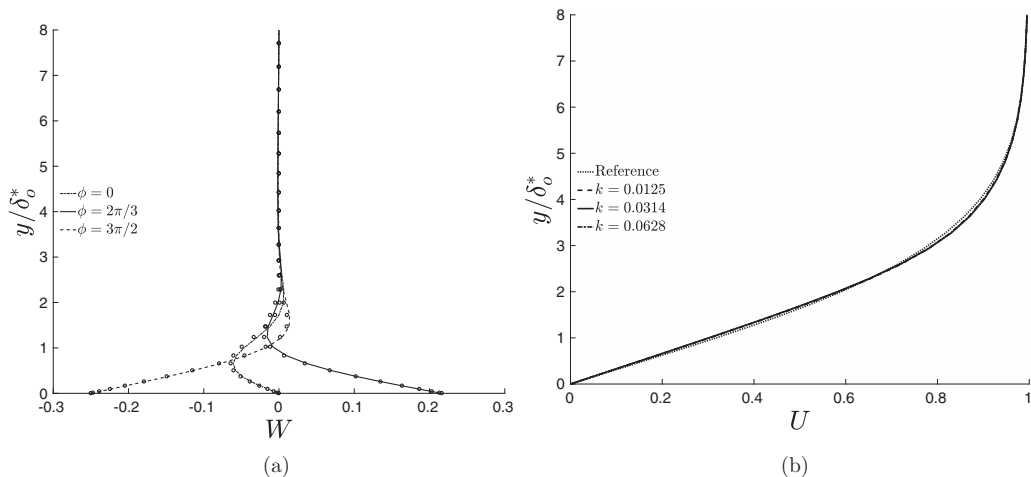


FIG. 15. (a) Stokes layer profile and (b) boundary layer profile at $x = 300$. “o” symbols in panel (a) are the solutions from the analytical equation (7), while the lines represent simulation results.

of penetration depth of the OSQ modes inside the boundary layer. The high-frequency modes are filtered out and have vanishing amplitude inside the boundary layer, while the low-frequency modes remain oscillatory deeper into the boundary layer. The Squire equation is thus selectively forced at the low-frequency end of the spectrum. The superposition of the generated Squire modes, which vanishes in the free stream, is nonzero inside the boundary layer. This “incomplete cancellation” of the Squire modes leads to the generation of vertical vorticity inside the boundary layer, consequently forming the low-frequency streaks.

In this framework, the Stokes layer can be seen to provide a secondary filtering within the boundary layer, which acts to further dampen the amplitude of the continuous OS modes that penetrate deep enough to reach the Stokes layer. This secondary filtering action causes the amplitude of (already diminished) continuous OS modes to further dampen inside the Stokes layer, providing negligible forcing for the generation of Squire modes. Thus, no streaks are seen within this region where the Stokes layer is active. Farther away from the wall, Stokes layer decays quickly, and the secondary filtering effect is lost and streaks consequently appear above the Stokes layer. Hack and Zaki [28] presented a similar result in a linearized study with time harmonic wall oscillations, where they show the emergence of a time-dependent filtering process in the presence of a periodic base flow which varied with the temporal Stokes layer height. In a subsequent study on temporal oscillations, the same authors [39] present an energy based analysis to show the weakening of the lift-up mechanism due to the redistribution of energy from wall-normal fluctuations to spanwise fluctuations.

TABLE II. Parameters of the low-frequency (A) and high-frequency (B) continuous OS modes introduced into the flow cases, where $(\alpha_N, \beta_N, \gamma_N)$ is the wave-number vector and Ω_N is the frequency.

Mode	\hat{v}	Ω_N	α_N	β_N	γ_N
A	2%	0.0112	$0.0112 + 0.00256i$	$\pm 0.0683 = 5 \times 2\pi/L_z$	0.656
B	1%	0.0225	$0.0225 + 0.00394i$	$\pm 1.09 = 8 \times 2\pi/L_z$	0.367

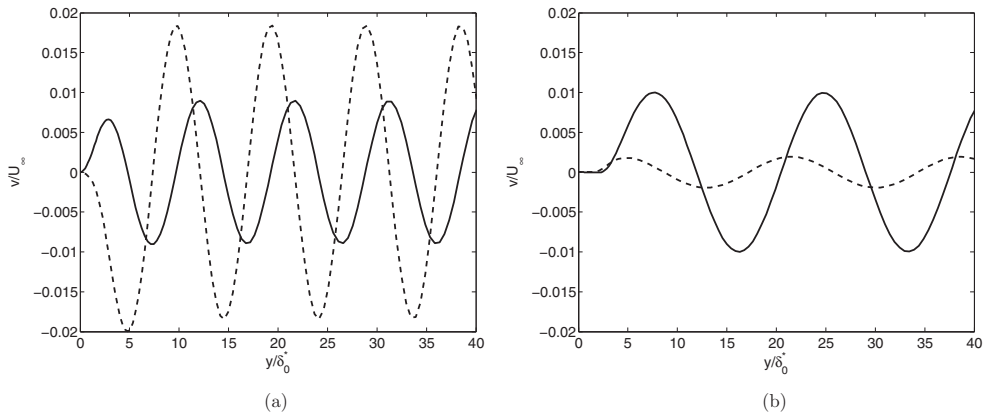


FIG. 16. Eigenfunctions for the (a) low-frequency penetrating mode A and (b) high-frequency nonpenetrating mode B at the inlet ($x = 0$). (—) Real part and (---) imaginary part.

VI. WALL CONTROL WITH TWO-MODE MODEL OF BYPASS TRANSITION

To further illustrate the filtering effect of the Stokes layer, simulations were carried out with the introduction of just a single Orr-Sommerfeld mode as in the bypass transition study of Schlatter *et al.* [24]. We mimic the simulation setup in Ref. [24] with the inlet Reynolds number based on displacement thickness being $Re_{\delta^*} = 350$, with the addition of control cases using spatial wall oscillations. The wave number used for the wall control is $k = 0.0314$ with an amplitude of $W_m = 0.5$. The computational domain based on the inlet δ^* is $1000 \times 60 \times 46$ in the streamwise, wall-normal, and spanwise directions. The simulation is performed using 360 and 60 Fourier modes in the streamwise and spanwise directions, together with 193 Chebyshev modes in the wall-normal direction. The fringe region is 90 units long at the end of the domain. The control region is implemented from $x_{\text{start}} = 100$ to $x_{\text{end}} = 900$. Free-stream modes introduced into the flow are shown in Table II where mode A is the low-frequency mode which penetrates deeper into the boundary layer, while mode B is the high-frequency mode which gets filtered by the boundary layer. The shape of the two modes at the inlet is shown in Fig. 16. Two simulations are performed with the introduction of just a single continuous OS mode (only mode A or only mode B) without any wall control. The results of the two simulations match those presented in Ref. [24] with the contours of u_{rms} being faithfully reproduced in Figs. 17(a) and 18(a).

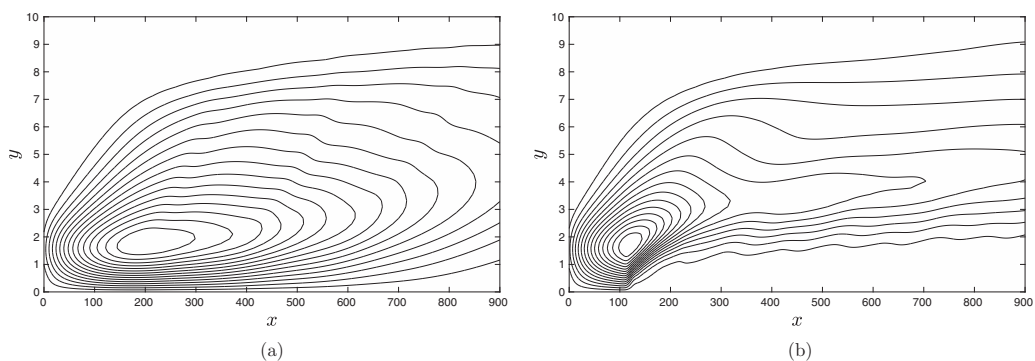


FIG. 17. A comparison of u_{rms} contours with and without wall control for a penetrating continuous OS mode (mode A). (a) No wall control and (b) Wall control.

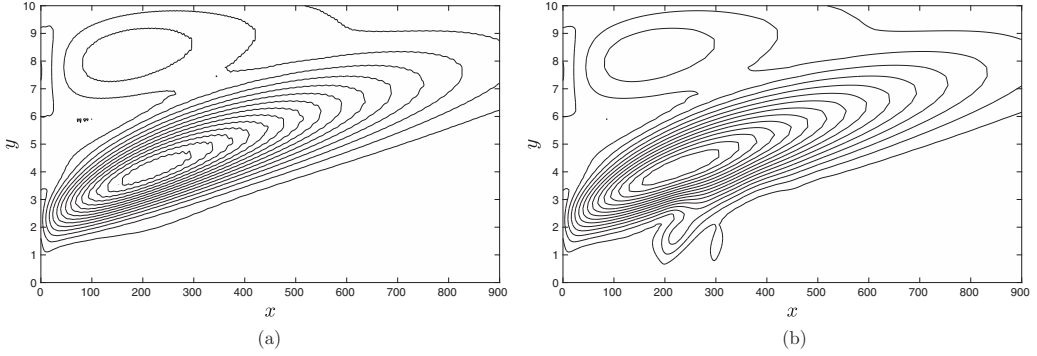


FIG. 18. A comparison of u_{rms} contours with and without wall control for a nonpenetrating continuous OS mode (mode B). (a) No wall control and (b) Wall control.

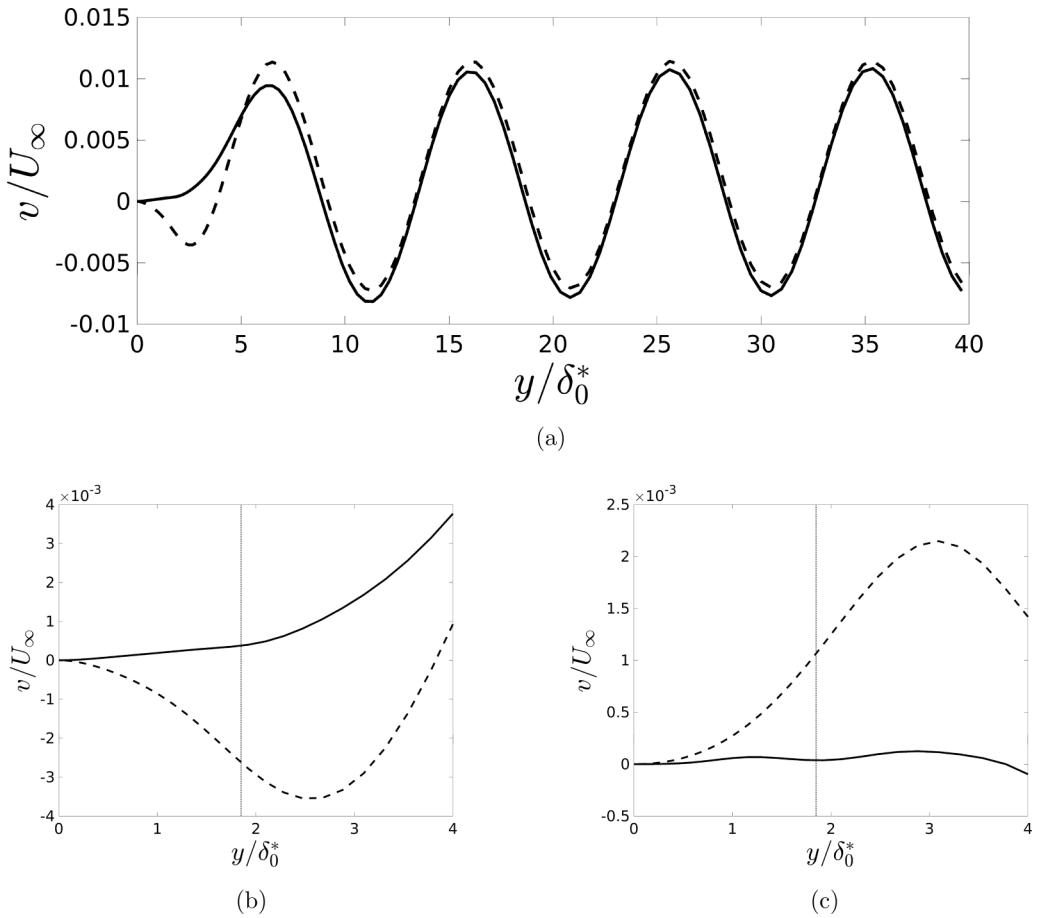


FIG. 19. Instantaneous wall-normal velocity profile at $t = 2000$ for the penetrating mode. (—) Cases with control and (---) cases without control. The vertical dotted line represents the approximate height where the oscillating spanwise velocity amplitude decays to $\approx 0.1W_m$. (a) Wall-normal velocity profile in the free stream at $x = 503$, (b) $x = 503$, and (c) $x = 747$.

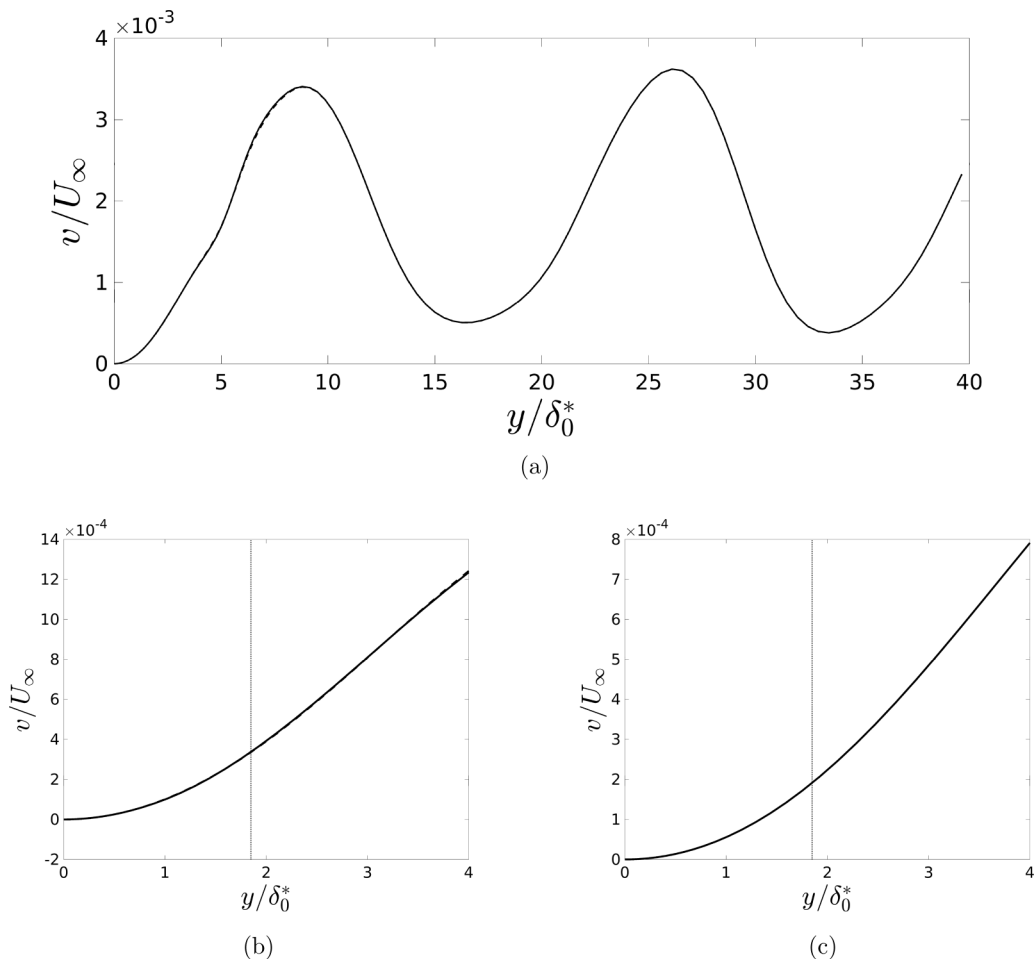


FIG. 20. Instantaneous wall-normal velocity profile at $t = 2000$ for a nonpenetrating mode. (—) Cases with control and (---) cases without control. The vertical dotted line represents the approximate height where the oscillating spanwise velocity amplitude decays to $\approx 0.1W_m$. (a) Wall-normal velocity profile in the free stream at $x = 503$, (b) $x = 503$, and (c) $x = 747$.

As clearly seen in Fig. 17, in the case of a penetrating continuous OS mode (mode A), the contours reach down to wall. However, when wall control is active, the contours of u_{rms} are lifted away from the wall with negligible streamwise fluctuation energy near the wall. For the case of a nonpenetrating continuous OS mode (mode B), the contours of u_{rms} do not reach down to the wall. Hence the flow remains almost unaffected by the presence of wall control, and the contours of u_{rms} for the wall control case are very similar to the case without wall control (Fig. 18).

The effect can also be seen in the instantaneous velocity fields. Figure 19 shows the instantaneous wall-normal velocity profile for the controlled and uncontrolled cases at $x = 503$ [Figs. 19(a) and 19(b)] and $x = 747$ [Fig. 19(c)] for the penetrating OS mode. In Fig. 19(a), the two profiles for the controlled and uncontrolled cases can be seen to nearly collapse away from the wall in the free stream. For the uncontrolled case the modulation of the wall normal velocity profile due to the continuous OS mode reaches down to wall as shown by the dashed lines. However, for the controlled case (solid line) the modulation dampens out just below the Stokes layer, which is approximately marked by the dotted vertical line. For a nonpenetrating mode the oscillations do not affect the

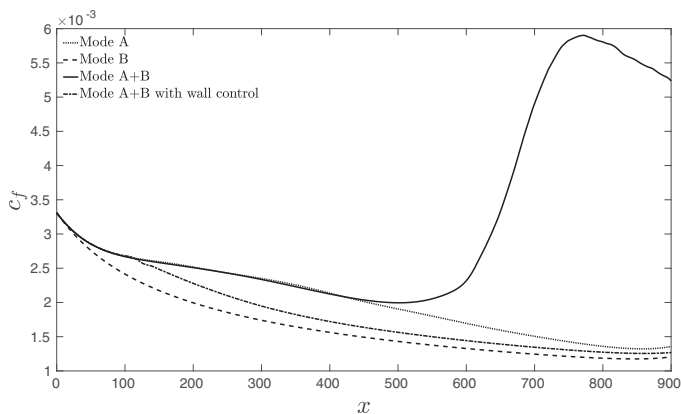


FIG. 21. c_f variation for different continuous OS modes in the flow.

mode shape substantially, with almost no deviations seen for the controlled case close to the wall (Fig. 20).

For the case when both the modes are present in the flow, the transition region is found to lie between $x = 400$ and $x = 800$ (Fig. 21), which is the same result reported in Ref. [24]. Introduction of spanwise wall oscillations causes the expected transition delay, and the flow does not undergo transition within the computational domain.

Wall oscillations thus affect only the low-frequency modes of the continuous OS spectrum which penetrate deep enough into the boundary layer. Since these modes are the ones responsible for streak formation in boundary layers, introduction of wall control in the form of spanwise wall oscillations hinders the streak formation mechanism. The mechanism, however, is not completely suppressed but remains active at a slightly higher wall-normal location, and thus streaks are seen to be lifted away from the wall. This interpretation explains why we see the peak fluctuations grow in the boundary layer (much before transition) even in the presence of wall control. With the onset of wall control, the near-wall fluctuations are dampened due to the action of secondary filtering provided by the Stokes layer. Thus initially the peak fluctuations decrease. As the damping saturates, the flow goes into a new state where the streaks are forming slightly away from the wall than in the uncontrolled case, and the process of streak formation (and growth) continues. It also explains why, despite nearly 90% reduction in peak fluctuations seen in some earlier studies [33,36] and 50% reduction observed in this current study, transition to turbulence is still observed via a bypass route. With 90% reductions of fluctuation intensity, a complete suppression of transition delay could be expected. However, the streak formation and growth mechanism is actually shifted to a higher wall-normal location, where streaks grow, break down, and transition to turbulence as a consequence.

Hence wall oscillations may not be capable of delaying transition to turbulence indefinitely despite linear studies showing very large suppression of peak velocity fluctuations. Of course, the spectral content of the FST affects the process of bypass transition [22], and special cases may possibly arise where transition to turbulence is suppressed completely.

VII. CONCLUSIONS

A wall control mechanism for delaying bypass transition using spatial and temporal wall oscillations is studied, and it is found that transition delay is possible for both types of wall oscillations. A coherent qualitative picture of the mechanism behind transition delay using oscillations of spanwise wall velocity has been built upon the framework of the continuous OS mode spectrum and the two-mode model of bypass transition.

Qualitatively, bypass transition can be reduced to the interaction of just two modes of the continuous OS spectrum: a low-frequency mode which penetrates into the boundary layer and causes the formation of near-wall streaks, and a high-frequency mode which gets filtered by the boundary layer but can interact with the streaks as they get lifted close to the boundary layer edge leading to streak breakdown and transition. In this particular framework, control of bypass transition can be done in one of two ways: modulating the low-frequency mode or modulating the high-frequency mode. Spanwise wall oscillations create a thin Stokes layer close to the wall within the laminar boundary layer. Thus, the control mechanism selectively affects the low-frequency modes while having a minimal effect on the high-frequency modes. The spanwise Stokes layer creates a secondary filter within the laminar boundary layer which dampens out the low-frequency modes close to the wall. This causes the OS mode amplitudes to diminish close to the wall, thus providing little forcing for the Squire modes. The Stokes layer, however, decays quickly away from the wall and the secondary filtering effect is lost. In this region within the boundary layer (which is above the Stokes layer), the OS modes continue to force the Squire modes, leading to the formation of streaks. Hence streak formation and growth continue at a slightly higher wall normal distance with a lower intensity. Once the streaks are generated at a higher wall normal location, spanwise wall control has little effect on the growth of streaks. The control mechanism therefore has only a finite capacity to delay bypass transition, which is why transition is still observed despite very high reductions in peak fluctuation intensities reported in linear studies [33] as well as in the case of a single generated streak [36].

Simulation with varying wave number (or frequency) and amplitude of wall oscillations shows a nonmonotonic behavior for both variables with the existence of an optimum amplitude for each wave number (or frequency) for maximum transition delay. Furthermore, the starting location of wall control affects the amount of transition delay that can be achieved with increased delay observed moving the start location upstream. However, the effect of this upstream movement of x_{start} saturates due to the fact that the transition process is now being governed by new streaks being formed above the Stokes layer where the wall control has little effect. Thereafter, little additional benefit, in terms of transition delay, is gained from extending the wall control region in the upstream direction.

ACKNOWLEDGMENT

The computations were partly performed on resources provided by the Swedish National Infrastructure for Computing (SNIC) at the PDC Center for High Performance Computing at the Royal Institute of Technology (KTH).

-
- [1] W. J. Jung, N. Mangiavacchi, and R. Akhavan, Suppression of turbulence in wall bounded flows by high-frequency spanwise oscillations, *Phys. Fluids A* **4**, 1605 (1992).
 - [2] R. Akhavan, W. Jung, and N. Mangiavacchi, Turbulence control in wall-bounded flows by spanwise oscillations, *Appl. Sci. Res.* **51**, 299 (1993).
 - [3] A. Baron and M. Quadrio, Turbulent drag reduction by spanwise wall oscillations, *Appl. Sci. Res.* **55**, 311 (1996).
 - [4] J.-I. Choi, C.-X. Xu, and H. J. Sung, Drag reduction by spanwise wall oscillation in wall-bounded turbulent flows, *AIAA J.* **40**, 842 (2002).
 - [5] K.-S. Choi, J.-R. Debisschop, and B. R. Clayton, Turbulent boundary-layer control by means of spanwise-wall oscillation, *AIAA J.* **36**, 1157 (1998).
 - [6] K.-S. Choi and M. Graham, Drag reduction of turbulent pipe flows by circular-wall oscillation, *Phys. Fluids* **10**, 7 (1998).
 - [7] C. A. Duque-Daza, M. F. Baig, D. A. Lockerby, S. I. Chernyshenko, and C. Davies, Modelling turbulent skin-friction control using linearized Navier-Stokes equations, *J. Fluid Mech.* **702**, 403 (2012).

- [8] D. Gatti and M. Quadrio, Reynolds-number dependence of turbulent skin-friction drag reduction induced by spanwise forcing, *J. Fluid Mech.* **802**, 553 (2016).
- [9] F. Laadhari, L. Skandaji, and R. Morel, Turbulence reduction in a boundary layer by a local spanwise oscillating surface, *Phys. Fluids* **6**, 3218 (1994).
- [10] S. Lardeau and M. A. Leschziner, The streamwise drag-reduction response of a boundary layer subjected to a sudden imposition of transverse oscillatory wall motion, *Phys. Fluids* **25**, 075109 (2013).
- [11] M. Quadrio and P. Ricco, Critical assessment of turbulent drag reduction through spanwise wall oscillations, *J. Fluid Mech.* **521**, 251 (2004).
- [12] P. Ricco, C. Ottonelli, Y. Hasegawa, and M. Quadrio, Changes in turbulent dissipation in a channel flow with oscillating walls, *J. Fluid Mech.* **700**, 77 (2012).
- [13] M. Skote, Turbulent boundary layer flow subject to streamwise oscillation of spanwise wall-velocity, *Phys. Fluids* **23**, 081703 (2011).
- [14] M. Skote, Temporal and spatial transients in turbulent boundary layer flow over an oscillating wall, *Int. J. Heat Fluid Flow* **38**, 1 (2012).
- [15] M. Skote, Comparison between spatial and temporal wall oscillations in turbulent boundary layer flows, *J. Fluid Mech.* **730**, 273 (2013).
- [16] M. Skote, Scaling of the velocity profile in strongly drag reduced turbulent flows over an oscillating wall, *Int. J. Heat Fluid Flow* **50**, 352 (2014).
- [17] E. Touber and M. A. Leschziner, Near-wall streak modification by spanwise oscillatory wall motion and drag-reduction mechanisms, *J. Fluid Mech.* **693**, 150 (2012).
- [18] C.-X. Xu and W.-X. Huang, Transient response of Reynolds stress transport to spanwise wall oscillation in a turbulent channel flow, *Phys. Fluids* **17**, 018101 (2005).
- [19] I. Yudhistira and M. Skote, Direct numerical simulation of a turbulent boundary layer over an oscillating wall, *J. Turbulence* **12**, N9 (2011).
- [20] C. Viotti, M. Quadrio, and P. Luchini, Streamwise oscillation of spanwise velocity at the wall of a channel for turbulent drag reduction, *Phys. Fluids* **21**, 115109 (2009).
- [21] M. Quadrio, P. Ricco, and C. Viotti, Streamwise-travelling waves of spanwise wall velocity for turbulent drag reduction, *J. Fluid Mech.* **627**, 161 (2009).
- [22] L. Brandt, P. Schlatter, and D. S. Henningson, Transition in boundary layers subject to free-stream turbulence, *J. Fluid Mech.* **517**, 167 (2004).
- [23] R. G. Jacobs and P. A. Durbin, Simulations of bypass transition, *J. Fluid Mech.* **428**, 185 (2001).
- [24] P. Schlatter, L. Brandt, H. C. de Lange, and D. S. Henningson, On streak breakdown in bypass transition, *Phys. Fluids* **20**, 101505 (2008).
- [25] T. A. Zaki and P. A. Durbin, Mode interaction and the bypass route to transition, *J. Fluid Mech.* **531**, 85 (2005).
- [26] P. Durbin and X. Wu, Transition beneath vortical disturbances, *Annu. Rev. Fluid Mech.* **39**, 107 (2007).
- [27] C. E. Grosch and H. Salwen, The continuous part of the Orr-Sommerfeld equation. Part 1: The spectrum and eigenfunctions, *J. Fluid Mech.* **87**, 33 (1978).
- [28] M. J. P. Hack and T. A. Zaki, The continuous spectrum of time-harmonic shear layers, *Phys. Fluids* **24**, 034101 (2012).
- [29] R. G. Jacobs and P. A. Durbin, Shear sheltering and the continuous spectrum of the Orr-Sommerfeld equation, *Phys. Fluids* **10**, 2006 (1998).
- [30] P. Andersson, L. Brandt, A. Bottaro, and D. S. Henningson, On the breakdown of boundary layer streaks, *J. Fluid Mech.* **428**, 29 (2001).
- [31] J. Mans, E. C. Kadijk, H. C. de Lange, and A. A. van Steenhoven, Breakdown in a boundary layer exposed to free-stream turbulence, *Exp. Fluids* **39**, 1071 (2005).
- [32] M. Dong and X. Wu, On continuous spectra of the Orr-Sommerfeld/Squire equations and entrainment of free-stream vortical disturbances, *J. Fluid Mech.* **732**, 616 (2013).
- [33] P. Ricco, Laminar streaks with spanwise wall forcing, *Phys. Fluids* **23**, 064103 (2011).
- [34] M. R. Jovanović, Turbulence suppression in channel flows by small amplitude transverse wall oscillations, *Phys. Fluids* **20**, 014101 (2008).

- [35] S. M. E. Rabin, C. P. Caulfield, and R. R. Kerswell, Designing a more nonlinearly stable laminar flow via boundary manipulation, *J. Fluid Mech.* **738**, R1-1 (2014).
- [36] P. S. Negi, M. Mishra, and M. Skote, DNS of a single low-speed streak subject to spanwise wall oscillations, *Flow Turbul. Combust.* **94**, 795 (2015).
- [37] S. Berlin, Oblique waves in boundary layer transition, Ph.D. thesis, Royal Institute of Technology (KTH), Stockholm, 1998.
- [38] M. Hack and T. A. Zaki, The influence of harmonic wall motion on transitional boundary layers, *J. Fluid Mech.* **760**, 63 (2014).
- [39] M. Hack and T. A. Zaki, Modal and non-modal stability of boundary layers forced by spanwise wall oscillations, *J. Fluid Mech.* **778**, 389 (2015).
- [40] M. Chevalier, P. Schlatter, A. Lundbladh, and D. S. Henningson, SIMSON—A pseudo-spectral solver for incompressible boundary layer flows, Technical Report TRITA-MEK 2007:07, KTH Mechanics, Stockholm, 2007.
- [41] P. Schlatter, S. Stolz, and L. Kleiser, LES of transitional flows using the approximate deconvolution model, *Int. J. Heat Fluid Flow* **25**, 549 (2004).
- [42] P. Schlatter, S. Stolz, and L. Kleiser, Large-eddy simulation of spatial transition in plane channel flow, *J. Turbulence* **7**, N33 (2006).
- [43] G. Eitel-Amor, R. Örlü, and P. Schlatter, Simulation and validation of a spatially evolving turbulent boundary layer up to $Re_\theta = 8300$, *Int. J. Heat Fluid Flow* **47**, 57 (2014).
- [44] P. Schlatter, S. Stolz, and L. Kleiser, Analysis of the SGS energy budget for deconvolution- and relaxation-based models in channel flow, in *Direct and Large-Eddy Simulation VI*, edited by E. Lamballais, R. Friedrich, B. J. Geurts, and O. Métais (Springer, Dordrecht, 2006), pp. 135–142.
- [45] P. Schlatter, E. Deusebio, L. Brandt, and R. de Lange, Interaction of noise disturbances and streamwise streaks, in *Seventh IUTAM Symposium on Laminar-Turbulent Transition*, edited by P. Schlatter and D. S. Henningson (Springer, Dordrecht, 2010), pp. 355–360.
- [46] P. Schlatter, E. Deusebio, R. de Lange, and L. Brandt, Numerical study of the stabilisation of boundary-layer disturbances by finite amplitude streaks, *Int. J. Flow Control* **2**, 259 (2010).
- [47] P. Schlatter, Direct numerical simulation of laminar-turbulent transition in boundary layer subject to free-stream turbulence, Diploma thesis, Royal Institute of Technology (KTH), Stockholm, 2001.
- [48] E. Kleusberg, Wind turbine simulations using spectral elements, Licentiate thesis, Royal Institute of Technology (KTH), Stockholm, 2017.
- [49] P. J. Schmid and D. S. Henningson, *Stability and Transition in Shear Flows*, Applied Mathematical Sciences Vol. 142 (Springer Science & Business Media, New York, 2012).